SPE 110778

Multiscale Methods for Modeling Fluid Flow Through Naturally Fractured Carbonate Karst Reservoirs

P. Popov, G. Qin, L. Bi, Y. Efendiev, R. Ewing, Institute for Scientific Computation, Texas A&M University; Z. Kang, J. Li, Research Institute of Petroleum Exploration and Development, SINOPEC Corporation, Beijing, P.R. China

This paper was prepared for presentation at the 2007 SPE Annual Technical Conference and Exhibition held in Anaheim, California, USA, 11–14 November, 2007.

Abstract

Modeling and numerical simulations of Carbonate Karst reservoirs is a challenging problem due to the presence of vugs and caves which are connected via fracture networks at multiple scales. In this paper we propose a unified approach to this problem by using the Stokes-Brinkman equations which combine both Stokes and Darcy flows. These equations are capable of representing porous media (porous rock) as well as free flow regions (fractures, vugs, caves) in a single system of equations. The Stokes-Brinkman equations also generalize the traditional Darcy-Stokes coupling without sacrificing the modeling rigor. Thus, it allows us to use a single set of equations to represent multiphysics phenomena on multiple scales. The local Stokes-Brinkman equations are used to perform accurate scale-up. We present numerical results for permeable rock matrix populated with elliptical vugs. Both constant and variable background permeability matrices are considered and the effect the vugs have on the overall permeability is evaluated. Fracture networks connecting isolated vugs are also studied. It is shown that the Stokes-Brinkman equations provide a natural way of modeling realistic reservoir conditions, such as partially filled fractures.

Introduction

Naturally fractured karst reservoirs presents multiple challenges for numerical simulations of various fluid flow problems. Such reservoirs are characterized by the presence of fractures, vugs and caves at multiple scales. Each individual scale is an ensemble of porous media, with well defined properties (porosity and permeability) and a free flow region, where the fluid (oil, water, gas) meets no resistance form the surrounding rock [1].

The main difficulty in numerical simulations in such reservoirs is the co-existence of porous and free flow regions, typically at several scales. The presence of individual voids such as vugs and caves in a surrounding porous media can significantly alter the effective permeability of the media. Furthermore, fractures and long range caves can form various types of connected networks which change the effective permeability of the media by orders of magnitudes. An additional factor which complicates the numerical modeling of such systems is the lack of precise knowledge on the exact position of the interface between the porous media (rock) and the and vugs/caves. Finally, the effects of cave/fracture fill in by loose material (sand, mud, gravel, etc), the presence of damage at the interface between porous media and vugs/caves and the roughness of fractures can play very important role in the overall response of the reservoir.

The modeling of fractured, vuggy media is traditionally done by using the coupled Stokes-Darcy equations [1, 2, 3, 4, 5, 6, 7, 8, 9, 10, 11]. The porous regions is modeled by the Darcy equation [4, 12], while the Stokes equation is used in the free flow region. At the interface between the two, various types of interface conditions are postulated [2, 3, 4, 5]. All of these interface conditions require continuity of mass and momentum across the interface. The difference comes when the tangential component of the velocities at the interface are treated. Each one of them proposes a different jump condition for the tangential velocities and/or stresses, related in some way to the fluid stress. The selection of jump condition is subject to the fine structure of the interface and the flow type and regime (c.f. e.g. [13] and the references therein). Furthermore, these jump conditions introduce additional media parameters that need to be determined. These parameters can be obtained either experimentally, or computationally.

There are several aspects of the coupled Darcy-Stokes approach, which make its application to vuggy reservoirs complicated. First, good knowledge is required both in the location of the porous/fluid interface as well as its fine-scale structure. Such precise information is hard to deduce from subsurface geological data. Secondly, there is need to obtain, numerically or experimentally values for parameters related to the interface conditions. Numerical determination is viable for engineered media, such as oil filters in the automotive industry, where the fine-scale porous geometry is known, either by design or can be obtained relatively easily, for example by 3D tomography. The experimental approach is more appropriate for subsurface formations, however, there are many difficulties associated with it. Finally, the free flow region which represents caves/vugs and fractures must be free of any obstacles such as loose fill-in material, and the fluid must also be free of any particle suspensions which are moving with it.

An alternative way of modeling vuggy media is to use the Stokes-Brinkman equations [1, 13, 14, 15, 16, 17, 18, 19]. These equations provide a unified approach in the sense that a single equation with variable coefficients is used for both porous and free-flow region. Stokes-Brinkman equations can be reduced to Stokes or Darcy equations by appropriate choice of the parameters. Since the different media types are distinguished by selecting the coefficients of the PDE, there is usually no need to formulate specific interface conditions. This is especially helpful in reservoir and groundwater flow, where the porous domain has a complicated topology. The numerical treatment of Stokes-Brinkman equation is simpler, due the lack of special interface conditions. Also, due to uncertainties associated with interface locations between vugs and the rock matrix, Stokes-Brinkman equations introduce a somewhat coarse model that does not require precise interface locations and avoid local grid refinement issues that are needed near the interfaces. Finally the Stokes-Brinkman equations provide a model that can be continuously varied from a Darcy dominated flow to a Stokes dominated flow, a feature which allows is to simulate effectively partially filled fractures or solid particles suspended in the fluid.

The two mathematical models for the fine scale: the Stokes-Darcy and the alternative proposed in this work, the Stokes-Brinkman model, are presented next. This is followed by a short discussion on the upscaling of the Stokes-Brinkman equation from the fine to the coarse scale. Two different types of numerical examples are presented. The first demonstrates that upscaling the Stokes-Brinkman model works for isolated vugs distributed in a porous matrix. The second class of examples deal with interaction between vugs and fracture networks.

Mathematical Models for Vuggy Media at Multiple Scales

We begin, by considering two scales, a fine and a coarse one. The fine scale media is composed of a porous region and a free flow region. The free flow region represents the vugs, caves and fractures. The porous region, which we will also refer to as matrix, has a much finer underlying structure of impermeable solid and pore space where fluid flow can occur. This fine scale structure is not considered but an effective response of the porous media is assumed governed by material parameters such as porosity and permeability.

At the coarse scale, on the other hand, the media is described mostly by Darcy flow. The fine scale features such as vugs caves and fractures, along with the surrounding porous matrix, are replaced by an effective material with well defined effective permeability and porosity. However certain features, such as, large, long-range caves (relative to the fine scale) may still be retained at the coarse scale. In the later situation, the Stokes-Brinkman model provides a very natural way of transiting between the scales.

To fix notation, the characteristic length scales of the fine and coarse scale, are denoted by l and L, respectively. Next, the usual small parameter ε is introduced [6, 20]:

$$\varepsilon = \frac{l}{L}. \tag{1}$$

Throughout this section, all quantities with superscript ε are defined on the fine scale, otherwise they are defined on the coarse scale. Let Ω^f be the free flow region, Ω^p the porous region and the interface between the two (excluding the external boundary) be Γ. Also, the fine scale fluid velocity is denoted by $\mathbf{v}^\varepsilon$ and the fine scale pressure by p^ε. In the free flow region, $\mathbf{v}^\varepsilon$ represents the actual physical velocity of the fluid but in the porous region it represents the Darcy (or averaged) velocity.

Darcy-Stokes The Stokes equation, used to describe the free flow region, has the form:

$$\nabla p^\varepsilon - \mu \Delta \mathbf{v}^\varepsilon = \mathbf{f} \qquad \text{in } \Omega^f, \tag{2}$$

$$\nabla . \mathbf{v}^\varepsilon = 0 \qquad \text{in } \Omega^f. \tag{3}$$

The first of these equation expresses the balance of linear momentum, and the second is the conservation of mass. Also, recall the fluid stress tensor $\boldsymbol{\sigma}$ is given by the formula:

$$\boldsymbol{\sigma} = -p\mathbf{I} + 2\mu\mathbf{D},$$

where $\mathbf{D}$ is the strain rate:

$$\mathbf{D} = \frac{1}{2}\left(\nabla \mathbf{v} + \nabla \mathbf{v}^T\right).$$

In the porous region, one has the classical Darcy law (c.f. e.g. [12, 6]), along with conservation of mass:

$$\mathbf{v}^\varepsilon = -\frac{\mathbf{K}}{\mu}\left(\nabla p^\varepsilon - \mathbf{f}\right) \qquad \text{in } \Omega^p, \tag{4}$$

$$\nabla . \mathbf{v}^\varepsilon = 0 \qquad \text{in } \Omega^p. \tag{5}$$

The two systems need to be coupled at the interface Γ. There are various ways in which this is achieved. For example, the classical condition of [2] states that:

$$[\mathbf{v}] \cdot \mathbf{n} = 0 \qquad \text{on } \Gamma, \tag{6}$$

$$2\mu \mathbf{D}\mathbf{n} = [p] \qquad \text{on } \Gamma, \tag{7}$$

$$\frac{\partial \mathbf{v}_f}{\partial \mathbf{n}} = \frac{\alpha_{BJ}}{\sqrt{K}} [\mathbf{v}] \cdot \mathbf{t}_i \qquad \text{on } \Gamma. \tag{8}$$

Here, $[\cdot]$ denotes the jump in a given quantity while moving from the fluid to the porous side, that is, form some field ϕ:

$$[\phi] = \phi_f - \phi_p,$$

$\mathbf{n}$ is a unit normal pointing from Ω^f to Ω^p and $\mathbf{v}_f$ is the velocity in the fluid region. In the above equations, the first interface condition (6) expresses conservation of mass across the interface, (7) expresses conservation of momentum, and (8) imposes a slip condition on the tangential component of the velocity. The dimensionless constant α_{BJ} is a material property which is representative of the microstructure (at much smaller scales than l) of the interface. It can be obtained either numerically, if such information is available or obtained experimentally.

It should be emphasized, that the exact form of the interface conditions (6)-(8) is an active area of research [2, 3, 4, 5, 8, 9, 10]. For example, [3] modified equation (8) to contain only variable in the fluid domain, [4, 5] studied the interface conditions based on the flow type, e.g. parallel or perpendicular to the interface [4, 5] and [8, 9, 10] studied the mathematical justifications of such interface conditions. The reader is referred to [13] for a detailed review.

The Stokes-Brinkman Equation Recall that the fine scale velocity is denoted by $\mathbf{v}^\varepsilon$ and the fine scale pressure by p^ε. The Stokes-Brinkman equation for a single phase flow in a porous/free flow media is written as follows (c.f. e.g. [14, 13]):

$$\mu \mathbf{K}^{-1}\mathbf{v}^\varepsilon + \nabla p^\varepsilon - \mu^* \Delta \mathbf{v}^\varepsilon = \mathbf{f} \qquad \text{in } \Omega, \tag{9}$$

$$\nabla . \mathbf{v}^\varepsilon = 0 \qquad \text{in } \Omega. \tag{10}$$

Here, $\mathbf{K}$ is a permeability tensor, which in Ω^p is equal to the Darcy permeability of the porous media, μ is the physical viscosity of the fluid and μ^* is an effective viscosity. The other two parameters - $\mathbf{K}$ and μ^* are selected differently depending on the media type (porous or free flow) and are discussed next. It will also be shown that, in the fluid region, $\mathbf{v}^\varepsilon$ represents the actual physical velocity of the fluid and in the porous region, it is the Darcy velocity.

The physical fluid viscosity μ is a material constant that defines the fluid under consideration (e.g. water, oil, etc) and is a uniform constant in the entire domain Ω. In the fluid region Ω^f, $\mathbf{K}$ is assumed to be ∞ and μ^* is taken equal to the physical fluid viscosity μ:

$$\mu^* = \mu, \qquad \mathbf{K} = \infty \qquad \text{in } \Omega^f \tag{11}$$

Observe that this selection of parameters implies that equations (9), (10) reduce to the Stokes system (2), (3).

In the porous region Ω^p, $\mathbf{K}$ is taken to be the Darcy permeability of the porous media. With that, and in the absence of distributed body force $\mathbf{f}$, equation (9) can be written as

$$\nabla p^\varepsilon = -\mu \mathbf{K}^{-1}\mathbf{v}^\varepsilon + \mu^* \Delta \mathbf{v}^\varepsilon \qquad \text{in } \Omega, \tag{12}$$

The reader will recognize that in the last equation, the only difference with Darcy's law (4) is the additional viscous term $\mu^* \Delta \mathbf{v}^\varepsilon$. So, if μ^* is taken equal to zero in Ω^p, then equation (9) reduces to (4). However this will reduce the Stokes-Brinkman system to the coupled Darcy-Stokes model. This will entail the difficulties mentioned previously, which we aim to avoid. Observe, that in most porous media, $\mathbf{K}$ is in the range of milli- to tens of Darcy. Thus, if μ^* is of the same order as the physical viscosity μ, that is

$$\mu^* \sim \mu$$

the term $\mu \mathbf{K}^{-1}\mathbf{v}^\varepsilon$ in equation (12) dominates by many orders of magnitude $\mu^* \Delta \mathbf{v}^\varepsilon$. Thus, the additional viscous term introduces only a small perturbation to Darcy's law. As a result the simplest possible choice for μ^* is

$$\mu^* = \mu$$

which, in complex geometries, uncertain interface location and lack of knowledge of the micro-scale interface features is a reasonable choice [13, pg. 26-29]. A different choice of μ^* is usually motivated by two factors. First, μ^* can be used to provide a more accurate model for the porous medium than is afforded by Darcy law [15, 17, 19]. Secondly, the effective viscosity μ^* can also be used to mimic various jump condition at the interface, as done by [16, 21]. The reader is again referred to [13, pg. 26-29], for an indepth discussion on this subject.

The Stokes-Brinkman equation offers several advantages. First, it allows a unified approach to the ensemble of porous and free-flow media by formulating a single equation in the entire domain Ω. The different media types are distinguished by proper selection of $\mathbf{K}$ and μ^* in equations (9), (10) and there is no need to formulate specific interface conditions, as in the coupled Darcy-Stokes approach. This is especially helpful when the porous domain Ω^p has a complicated topology, as is the case in vuggy reservoirs. The unified approach also translates to significant simplification in the numerical treatment of equations (9), (10).

Upscaling As was mentioned earlier, vuggy, fractured reservoirs feature multiple scales, and upscaling is necessary for numerical simulation at the field scale. In this section, we consider the upscaling of the Stokes-Brinkman equation from the fine to the coarse scale.

First, we assume that we have a REV which features both porous and fluid domains. In this case, the coarse scale equations are Darcy law and conservation of mass. The short summary presented next is based on two-scale asymptotic expansion [6, 20]. The procedure is very similar to the one employed for upscaling the Stokes equation in an impermeable porous media. The reader is thus referred to [22] for technical details. The results are summarized next. A formal asymptotic expansion of the type

$$\mathbf{v}^{\varepsilon}(\mathbf{x}) = \mathbf{v}_{-2}(\mathbf{x},\mathbf{y}) + \varepsilon \mathbf{v}_{-1}(\mathbf{x},\mathbf{y}) + \varepsilon^2 \mathbf{v}_0(\mathbf{x},\mathbf{y}) + \varepsilon^3 \mathbf{v}_1(\mathbf{x},\mathbf{y}) + \dots \tag{13}$$

$$p^{\varepsilon}(\mathbf{x}) = p_0(\mathbf{x},\mathbf{y}) + \varepsilon p_1(\mathbf{x},\mathbf{y}) + \dots \tag{14}$$

is substituted in equations (9), (10). By further assuming that

$$\mu \mathbf{K}^{-1} \geq \mathcal{O}\left(\varepsilon^{-2}\right), \tag{15}$$

one obtains that the first two velocity terms $\mathbf{v}_{-2}$ and $\mathbf{v}_{-1}$ are identically zero and the first term in the pressure expansion p_0 does not depend on the fine-scale variable $\mathbf{y}$, that is $p_0 = p_0(\mathbf{x})$.

Next, one obtains a set of cell problems that are used to compute the effective (or upscaled) permeability of the REV. Let d be the dimension (2 or 3) and $\mathbf{e}_i$ be a unit vector in the i-th direction. The d cell problems needed to upscale the Stokes-Brinkman equation are:

$$\mathbf{K}^{-1}\mathbf{w}^i + \nabla_{\mathbf{y}} q^i - \frac{\mu^*}{\mu}\Delta_{\mathbf{y}}\mathbf{w}^i = \mathbf{e}_i \qquad \text{in } Y, \tag{16}$$

$$\nabla_{\mathbf{y}} \cdot \mathbf{w} = 0 \qquad \text{in } Y. \tag{17}$$

Here, $\mathbf{w}^i$ are Y-periodic and the (fine-scale) pressure q has zero average in Y. The permeability is then computed by averaging the fine-scale velocities:

$$K_{ij} := \langle {w_i}^j \rangle_Y = \frac{1}{|Y|}\int_Y w_i d\mathbf{y}. \tag{18}$$

The macroscopic (upscaled) flux is given by the Darcy's law:

$$\langle \mathbf{v}^{\varepsilon} \rangle = -\frac{\mathbf{K}}{\mu}\left(\nabla \langle p^{\varepsilon} \rangle - \mathbf{f}\right), \tag{19}$$

and subject to conservation of mass:

$$\nabla . \langle \mathbf{v}^{\varepsilon} \rangle = 0. \tag{20}$$

Note that $\mathbf{w}^i$, $i = 1, ..., d$ are the fine-scale velocities in the REV, that is Y, are subject to unit forcing in the respective direction. Since $\mathbf{e}_i$ can also be transferred to the pressure term:

$$\nabla\left(\mathbf{q}^i + x_i\right) = \nabla \mathbf{q}^i + \mathbf{e}_i,$$

one can consider $\langle \mathbf{w}^i \rangle$ as the averaged flux in Y over a unit pressure drop in the i-th coordinate direction.

The above upscaling works well under the assumption (15) and that an REV consisting of both porous and fluid region exists. Assumption (15) is quite general, since typically $\mathbf{K}^{-1}$ dominates the fluid viscosity by orders of magnitude. When $\mathbf{K} \sim \varepsilon^2 \mu$ the Brinkman term in the porous part of equation (16) is significant. The fine-scale velocities in the porous and fluid region will be of similar orders and noticeable mass transfer will occur between the fluid and solid, regardless of the flow regime. When $\mathbf{K} \ll \varepsilon^2 \mu$, the Brinkman term in (16) will dominate in the porous part of Y. As a result, the flow will significantly depend on the geometry of the REV. For example, in the case of connected vugs, the flow trough the vugs will dominate any flow in the porous part and one will essentially be homogenizing Stokes flow in impermeable media.

It is also possible that the some regions of the fine-scale domain do not allow upscaling, for example when an REV contains only a fluid part. This will happen if there are fluid regions with characteristic size much larger then l, c.f. equation (1). In such cases one can upscale the part of the fine scale where suitable mixture of porous media and vugs exist. Large scale voids on the other hand can be retained as free flow regions at the coarse scale. Then one will have a homogenized Stokes-Brinkman equation on the coarse scale, where the fluid region is represented by vugs, caves or fractures that cannot be homogenize. The porous region is the part susceptible to homogenization. There, the macroscopic velocity and pressure are defined as the average of the respective fine-scale quantities. In this way, the Stokes-Brinkman model allows us to upscale fractured, vuggy media, in a natural way and retaining the same equation at all scales. This allows successive homogenization at multiple scales.

Numerical Experiments

Discretization In order to solve numerically the fine-scale problem (9), (10), as well as the cell problems (16), (17) we use a mixed finite element method for the Stokes-Brinkman equations in the primary variables. We use Taylor-Hood elements (continuous quadratic velocity and continuous linear pressure, for more details, see e.g. [23]) on unstructured grids. The Taylor-Hood element is one of the few commonly used elements for the Stokes equation which is also stable for the Stokes-Brinkman equation [24]. It also provides a good approximation for both velocity and pressure.

The linear systems resulting from this finite element discretization are symmetric and indefinite and are solved using preconditioned conjugate gradient method for the pressure Schur complement. For more details on these types of numerical the reader is referred to [23]. The coarse-scale problems (19), (20) are solved by standard, conforming finite element method (c.f. e.g. [25]).

Upscaling of randomly distributed, disconnected vugs In this section we perform numerical examples designed to test the upscaling of the Stoke-Brinkman equations. We consider a fine scale domain populated with randomly distributed ellipsoidal vugs, shown in Figure 1(a). The vugs are generally well separated from each other and not connected. The objective is to compare a fine-scale reference solution of equations (9), (10) with the coarse scale model (19), (20).

Two numerical examples are computed. In both examples the fluid under consideration was water ($\mu = 1cP$). In the first example the background permeability was taken homogeneous in order to understand the effect of the vugs.

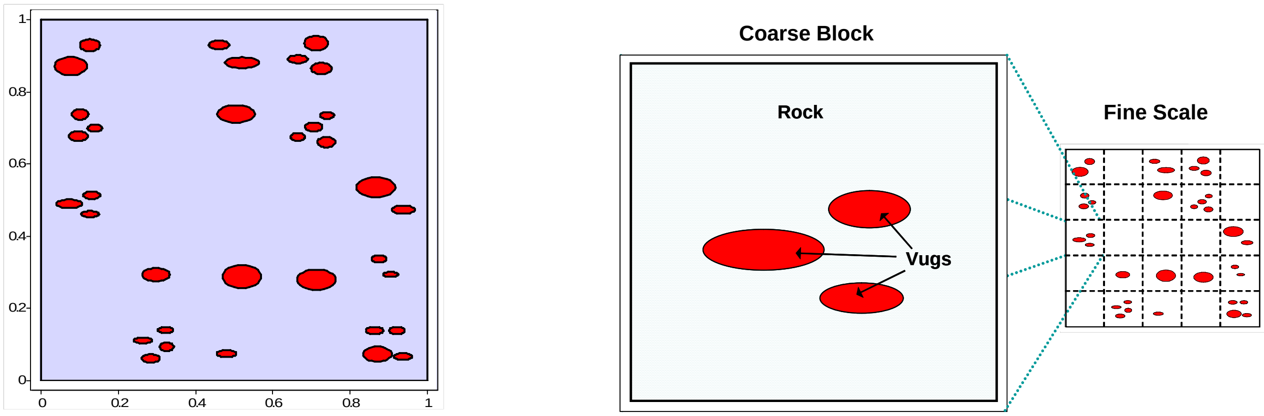

(a) Fine-scale domain (b) 5×5 Coarse block partitioning

Figure 1: Fine scale domain (a) consisting of porous rock and randomly distributed elliptical vugs (red). The coarse block partitioning used for upscaling calculations is shown to the right (b).

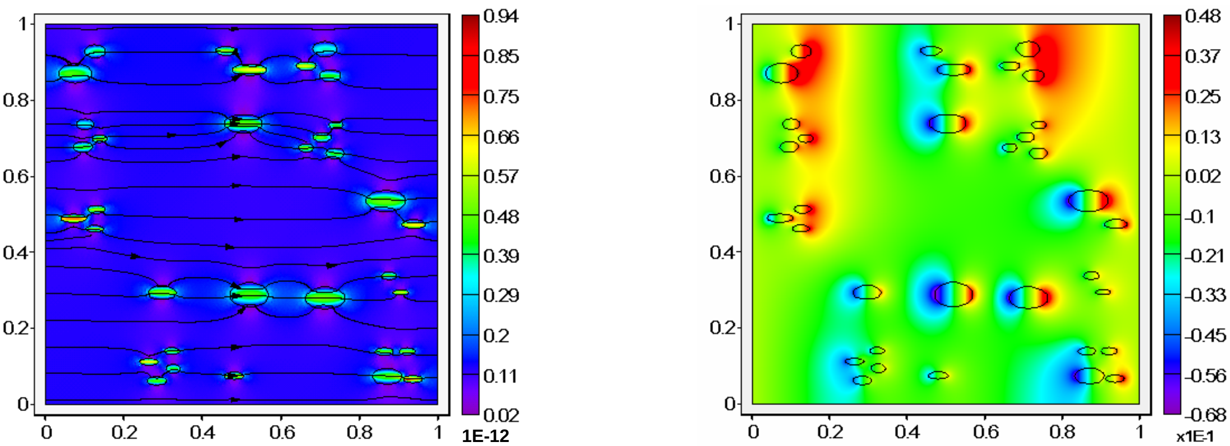

(a) Streamlines and velocity magnitude (b) Variation in the pressure (plotted is $p - (1 - x)$)

Figure 2: Fine scale reference solution (homogeneous matrix permeability)

In the second example, a variable background permeability field was considered.

Homogeneous matrix permeability In the first example, the background permeability field is homogeneous with $K = 1mD$. We consider no flow at top and bottom sides of the domain (Figure 1(a)). The flow is driven by a unit pressure drop in the horizontal (x) direction. This is achieved by setting a $1Pa$ pressure at the left side and zero at the right side of the domain. The fine scale solution is shown in Figure 2.

Next, the whole domain is divided into 5×5 coarse grid blocks, as shown in Figure 1(b). For each coarse grid, the upscaled permeability is computed (c.f. the cell problems (16), (17)). The horizontal component K_{11} of the permeability tensor $\mathbf{K}$ is shown in Figure 3(a). We observe from this figure that in the coarse regions with high concentration of vugs, the upscaled permeability is higher. In Figure 3(b), we plot the corresponding coarse-scale pressure. We have compared this coarse-scale pressure with the averaged coarse-scale pressure obtained from fine-scale solution. The relative L_2 error was found to be less than 2% and there is no visual difference in the plots. For this reason, we do not present the plot of averaged fine-scale pressure field. This result suggests that the proposed upscaling method provides accurate coarse-scale solution for homogeneous background permeability field.

Variable matrix permeability In these numerical tests a heterogeneous, isotropic background permeability, as shown in Figure 4(a), is considered. The vug population (size, shape and locations) are identical to the previous example (Figure 1(a)). The fine-scale matrix permeability field is a realization of a stochastic field with prescribed overall variance (quantified via σ^2, the variance of $\log(k)$), correlation structure and covariance model. It was generated using the GSLIB algorithms [26], characterized by a spherical variogram. The field has long correlation length in the horizontal direction (0.4) and smaller in the vertical direction (0.1). The boundary conditions are the same as in the previous example.

In Figures 4(b), 4(c), the fine-scale solution is plotted for velocity and pressure fields. We see from this figure that the heterogeneous permeability field creates additional high flow channels for the vugs which enhances the connectivity of the media. This is more evident if

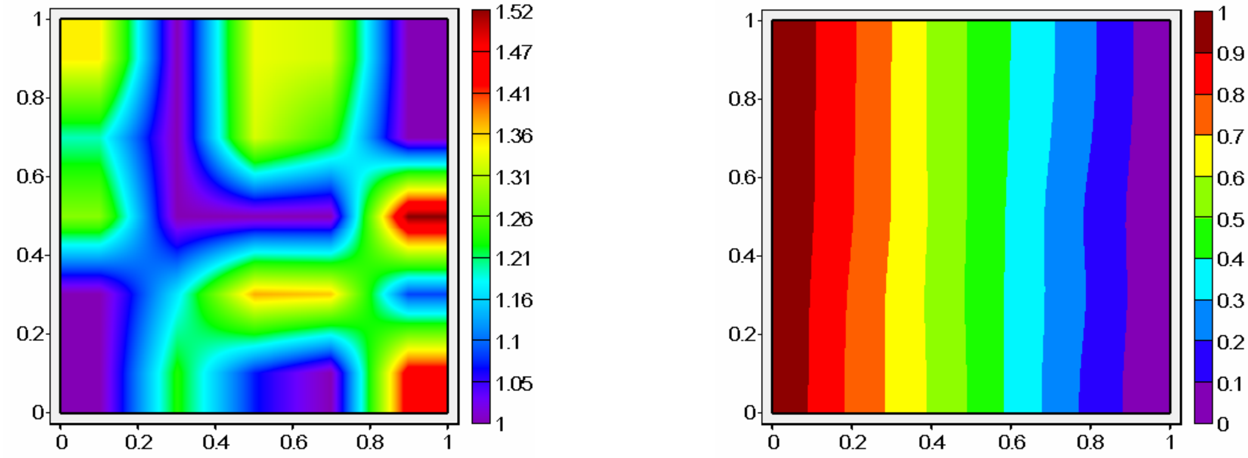

(a) K_{11} (in mD)

(b) Coarse-scale Pressure

Figure 3: Upscaled permeability (left) corresponding coarse-scale pressure (right).

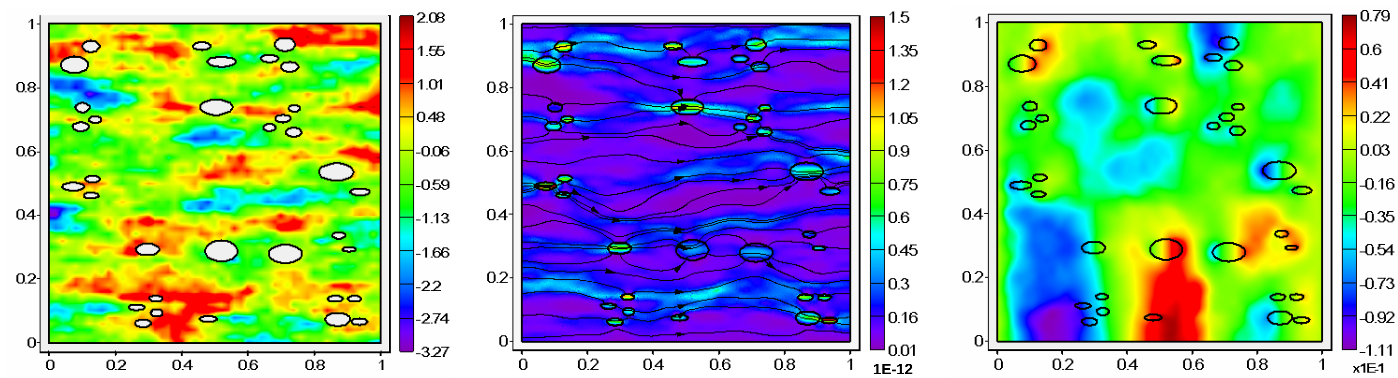

(a) Fine scale permeability (log plot)

(b) Streamlines and velocity magnitude

(c) Variation in the pressure $(p - (1 - x))$

Figure 4: Heterogeneous fine-scale permeability and reference solution. The background permeability field used at the fine scale is shown to the left (a). This is a log plot, the actual permeability is $k = C \exp(\cdot)$, where C is selected so that the average of k is $1 mD$. The reference solution (b), (c), obtained by the Stokes-Brinkman model.

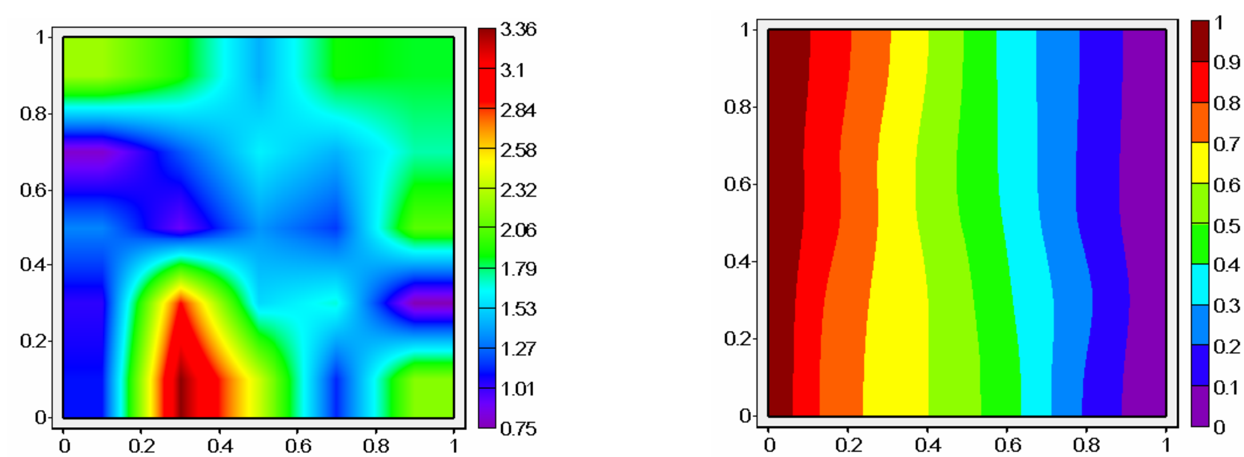

(a) K_{11} (in mD)

(b) Coarse-scale pressure

Figure 5: Upscaled permeability (left) corresponding coarse-scale pressure (right).

one compares Figure 2(a) and Figure 4(b). The presence of background heterogeneous permeability field alters the streamlines significantly.

The upscaling was performed on the same 5×5 coarse grid (Figure 1(b)), as in the previous example. Comparing Figure 3(a) and Figure 5(a), one can also observe that the upscaled permeabilities are quite different for homogeneous and heterogeneous background permeabilities. The highest permeability in the case of heterogeneous background permeability is $3.36mD$, while the highest permeability in the case of homogeneous background permeability is only $1.52mD$. Moreover, one can also observe different pattern structure in the graphs of upscaled permeabilities.

The upscaled pressure is computed using upscaled permeabilities, and the result is depicted in Figure 5(b). Again, we compared the upscaled pressure with averaged fine-scale pressure and the relative L_2 error is less than 5% and there is no visual difference between two plots. This result again suggests that the proposed upscaling method provides accurate coarse-scale solution for heterogeneous background permeability field.

Vugs and Fracture Networks In this section, we study the interaction between vugs and fracture networks. The effective permeability of a coarse block is computed for two different types of fracture networks connecting large vugs. The effects of fracture fill-in are also studied.

Effects of vugs connected by fractures A coarse block with three large elliptical vugs imbedded inside the block (REV) is considered. A fracture network connecting the vugs as well as the boundary of the REV is established. Three cases were considered:

- *Case I*: The effective permeability tensor $\mathbf{K}$ for the entire block was computed ignoring all the fractures (Figure 6(a)).
- *Case II*: The three fractures connecting the vugs were included in the computation, but the two cracks connecting the vugs to the boundary of the REV were not included (Figure 6(b)).
- *Case III*: All the fractures were included in the simulation (Figure 6(c)).

The simulations were set-up as follows: The coarse block with dimensions $20 \times 20m$ was used in all simulations. The matrix had a uniform permeability of $\mathbf{K}_r = 1mD$. The fractures were straight and had aperture in the range $1.1 - 1.7cm$. They also were assumed to have completely smooth surface. When a fracture was included in the simulation, it was treated as a free flow region ($\mathbf{K} = \infty$). When a fracture was not included in a simulation it was assigned the same permeability as the surrounding rock matrix.

The results of the simulations are presented in Table 1. As expected, *Case I* is similar to the upscaling calculations of the precious section. The upscaled permeability increased by $70\% - 90\%$ compared to the background matrix permeability.

The calculation of *Case II* show that connecting the vugs by short-range fractures of centimeter size nearly doubled the effective permeability in the horizontal direction in comparison to the basic *Case I*. The vertical permeability grew by another 20%. The larger increase in horizontal permeability is probably due to the fact that two of the three fractures run in that direction. Also, while having big effect, the effective permeability remained of the same order as the background matrix permeability ($1mD$). This can be easily explained by realizing that the fluid cannot enter the vugs directly but needs to pass through the matrix, thus the matrix determines the order of magnitude of the overall permeability.

The results for *Case III* show permeability about six to seven orders of magnitude more than the background, matrix permeability. This implies that most of the flow runs directly trough the fractures and the matrix contributes very little to the overall flow rate. Note also that the off-diagonal components are non-zero. This is due to the fact the REV is not completely symmetric. These results raise two important questions. First, how to upscale REVs in the presence of long range fractures. And, secondly, what other physical effects become important in such situations.

Modeling of Fracture Fill-in There are several factors that were not included in computing the effective permeability of a coarse block with vugs interconnected by long-range fracture networks. First, the fractures are never straight line, but instead have complex shape. Moreover, the fractures aperture is not constant, but can vary along the length of the fracture. In places a fracture may nearly close, due to local roughness of its surface. Secondly, the fracture itself need not be a completely free-flow area, but instead may have various types of filling, such as mud, sand, gravel, etc. Both of these factors may alter the flow rate trough a fracture by orders of magnitude. Additionally, the fluid itself may have significant amount of suspended solid particles, which may alter the flow in a fracture.

In this section we address the problem of modeling fracture fill-in by means of the Stokes-Brinkman model. As was mentioned earlier, the permeability of a free flow region is set to ∞ (c.f. equation (11)). However, in the case of fracture fill-in (partial or full) one may assign a finite permeability of the fracture. Depending on the type of the fill-in, the flow in the fracture may resemble Stokes flow (high porosity fill-in) or Darcy flow (low porosity fill-in). Thus, if the permeability of the fill-in material is known one may assign a finite permeability in the fracture and perform the scale-up.

To investigate the effects of finite permeability in a filled fracture, we performed a number of numerical simulation. The geometry under consideration was that of *Case III* of the previous section (Figure 6(c)). The basic matrix permeability was taken to be $1D$. The permeability of the fractures K_f (all five of them) were assigned several different permeabilities, ranging from the matrix perme-

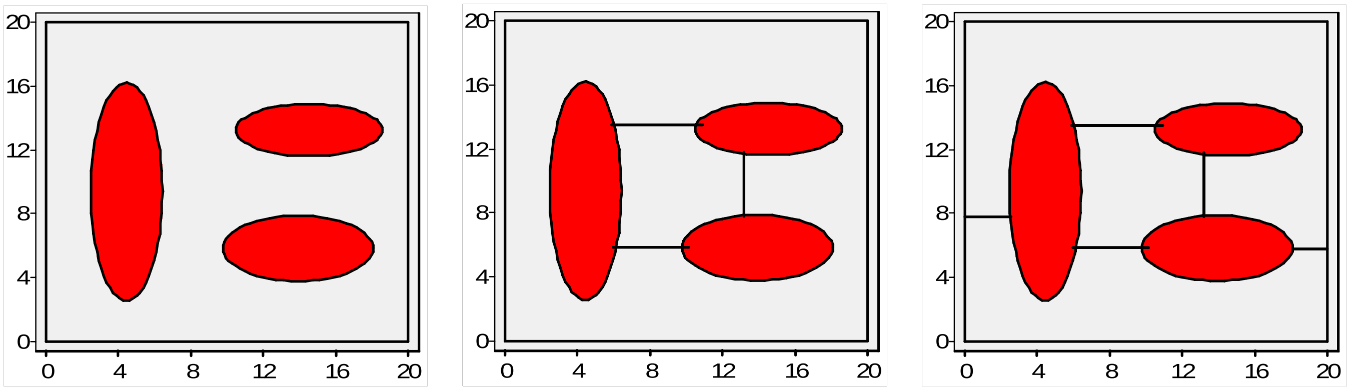

(a) *Case I*: Disconnected Vugs

(b) *Case II*: Short range fractures connecting the vugs

(c) *Case III*: Short and long range fractures running through the vugs and REV

Figure 6: Representative cases of vugs and fracture networks.

Table 1: Effective permeabilities for a coarse block with vugs connected by a fracture network.

	Case I	Case II	Case III
Effective Permeability Tensor (mD)	$\begin{pmatrix} 1.72 & 0.0 \\ 0.0 & 1.92 \end{pmatrix}$	$\begin{pmatrix} 3.35 & 0.0 \\ 0.0 & 2.37 \end{pmatrix}$	$\begin{pmatrix} 13.2 & -1.35 \\ -1.35 & 0.14 \end{pmatrix} \times 10^6$

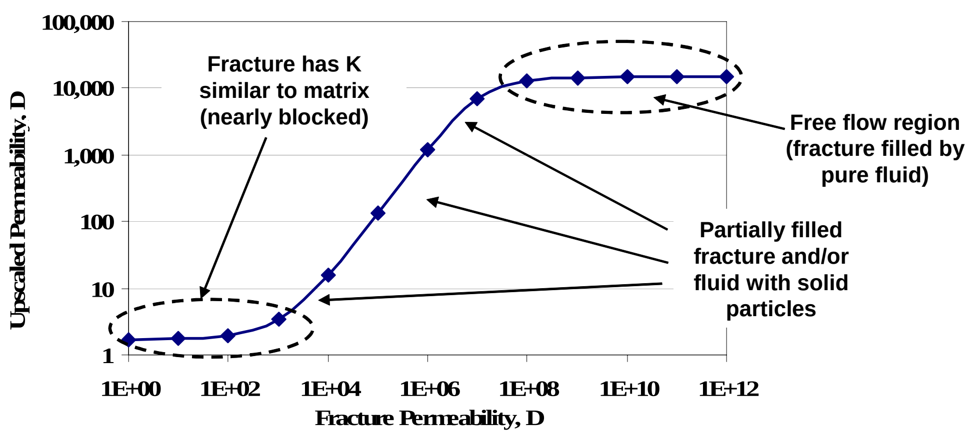

Figure 7: Effective permeability (K^*_{11} component) of the coarse block as a function of the fracture permeability

ability $1D$ to ∞. The vugs were always maintained free flow regions, that is, the permeability there was ∞.

The effective permeability $\mathbf{K}^*$ of the entire block was computed for each value of K_f. The results are shown in Figure 7. At the left most end of the graph, the fracture permeability K_f is equal to that of the matrix, that is the fractures are completely blocked. It can be seen that K_f needs to increase by a factor of 100, before a significant change in $\mathbf{K}^*$ occurs. The region in the right part of the graph on the other hand, is the free, or nearly free flow region. This flow regime starts at around $K_f \sim 10^8 - 10^9 D$ and an increase in K_f past that range does not visibly change $\mathbf{K}^*$. There is a large (six orders of magnitude), intermediate range of values of K_f $(10^2 - 10^8 D)$, where the effective permeability changes smoothly form the low perm limit (blocked fracture) to the high perm limit (unobstructed fracture). Since the difference in $\mathbf{K}^*$ between blocked, or equivalently, no fractures at all, and unobstructed fracture is many orders of magnitude, determining the permeability of the fill in material becomes an important task.

Conclusions

The results of Section demonstrate that a fine-scale model based on Stokes-Brinkman equations can be used to describe the flow through vugular porous media. Our upscaled results show that the heterogeneous background permeability field can give very different results compared to homogeneous background permeability with the same vug locations. In particular, the presence of high permeability channels connecting the vugs can increase substantially the overall permeability. The numerical tests also show that the proposed upscaling to Darcy law at the coarse scale is accurate in the case of isolated vugs.

The results of Section demonstrate that the presence of short-range fracture network connecting large vugs can change the effective permeability of a coarse block by a factor of 2-4. However, the effective permeability remains of the same order of magnitude and upscaling such media poses no challenges. On the other hand, long range, large aperture, fractures, may change the effective permeability by many orders of magnitude. In such cases secondary effects, such as fracture fill-in and roughness become important and need to be included in the fine-scale simulations. If the fractures are unobstructed and the resulting effective permeability is very high it may be necessary to consider more complex coarse-scale models which involve near well modeling and/or iterative homogenization as done by [27, 28].

It was also shown, that the Stokes-Brinkman equations allow the simulation of high porosity, but finite permeability fill-in regions in fractures and caves in a natural way. This feature of the Stokes-Brinkman model can be extended to also capture uncertainty in the interface location, damage zones near the interface and particle suspension in the working fluid.

References

1. Hornung, U.: *Homogenization and porous media*, Interdisciplinary Applied Mathematics. 6.New York, Springer (1997).
2. Beavers, G. and Joseph, D.: "Boundary Conditions at a Naturally Permeable Wall," (1967) **30**, 197.
3. Saffman, P.: "On the boundary condition at the surface of a porous medium." *Studies appl. Math.* (1971) **50**, 93.
4. Sanchez-Palencia, E. and Ene, H.: "Equations et phénomènes de surface pour l'écoulement dans un modèle de milieu poreux," *Journal de Mécanique* (1975) **14**, 73.
5. Levy, T. and Sánchez-Palencia, E.: "On boundary conditions for fluid flow in porous media," *Internat. J. Engrg. Sci.* (1975) **13**, 923.
6. Sanchez-Palencia, E.: *Non-Homogeneous Media and Vibration Theory*, volume 127 of *Lecture Notes in Physics*, Springer-Verlag, Berlin (1980).
7. Kaviany, M.: *Principles of Heat Transfer in Porous Media*, Mechanical Engineering Series, Springer-Verlag, New York (1999).
8. Jäger, W. and Mikelić, A.: "On the boundary conditions at the contact interface between a porous medium and a free fluid," *Ann. Scuola Norm. Sup. Pisa Cl. Sci. (4)* (1996) **23**, 403.
9. Jäger, W. and Mikelić, A.: "On the interface boundary condition of Beavers, Joseph, and Saffman," *SIAM J. Appl. Math.* (2000) **60**, 1111.
10. Jaeger, W., Mikelic, A. and Neuss, N.: "Asymptotic analysis of the laminar viscous flow over a porous bed," *SIAM J. Sci. Comput.* (2001) **22**, 2006.
11. Arbogast, T. and Lehr, H.L.: "Homogenization of a Darcy-Stokes system modeling vuggy porous media," *Comput. Geosci.* (2006) **10**, 291.
12. Darcy, H.: *Les fontaines publique de la ville de Dijon*, Librairie des Corps Impériaux des Ponts et Chaussées et des Mines, Paris (1856).
13. Laptev, V.: *Numerical solution of coupled flow in plain and porous media*, Ph.D. thesis, Technical University of Kaiserslautern, Germany (2003).
14. Brinkman, H.C.: "A Calculation of the Viscous Force Exerted by a Flowing Fluid on a Dense Swarm of Particles," *Applied Scientific Research Section A-Mechanics Heat Chemical Engineering Mathematical Methods* (1947) **1**, 27.
15. Lundgren, T.S.: "Slow flow through stationary random beds and suspensions of spheres," *Journal of Fluid Mechanics* (1972) **51**, 273.
16. Neale, G. and Nader, W.: "Practical Significance of Brinkmans Extension of Darcys Law - Coupled Parallel Flows Within a Channel and a Bounding Porous-Medium," *Canadian Journal of Chemical Engineering* (1974) **52**, 475.
17. Koplik, J., Levine, H. and Zee, A.: "Viscosity renormalization in the Brinkman equation," *Physics of Fluids* (oct 1983) **26**, 2864.
18. Allaire, G.: "Homogenization of the Navier-Stokes equations and derivation of Brinkman's law," *Mathématiques appliquées aux sciences de l'ingénieur (Santiago, 1989)*, Cépaduès, Toulouse (1991) 7–20.
19. Martys, N., Bentz, D.P. and Garboczi, E.J.: "Computer simulation study of the effective viscosity in Brinkman's equation," *Physics of Fluids* (apr 1994) **6**, 1434.
20. Zhikov, V., Kozlov, S. and Oleinik, O.: *Homogenization of Differential Operators and Integral Functionals*, Springer-Verlag, Berlin (1994).
21. Sahraoui, M. and Kaviany, M.: "Slip and no-slip velocity boundary conditions at interface of porous, plain media," *International Journal of Heat and Mass Transfer* (1992) **35**, 927.
22. Ene, H.: "Application of the Homogenization Method to Transport in Porous Media," *Dynamics of Fluids in Hierarchical Porous Media*, ed. J. Cushman, Academic Press, London (1990) 223–241.
23. Turek, S.: *Efficient Solvers for Incompressible Flow Problems: An Algorithmic and Computational Approach*, Springer Verlag, New York (1999).
24. Burman, E. and Hansbo, P.: "A unified stabilized method for Stokes' and Darcy's equations," *Journal of Computational and Applied Mathematics* (2007) **198**, 35.
25. Ciarlet, P.: *The Finite Element Method for Elliptic Problems*, number 40 in Classics in Applied Mathematics, SIAM, Philadelphia (2002).
26. Deutsch, C. and Journel, A.G.: *GSLIB: Geostatistical software library and users guide*, New York, 2 edition (1998).
27. Wu, Efendiev, Y. and Durlofsky, L.: "Analysis of upscaling absolute permeability," *Discrete Contin. Dyn. Syst., Ser. B* (2002) **2**, 185.
28. Efendiev, Y. and Pankov, A.: "Numerical homogenization of monotone elliptic operators," *Multiscale Modeling and Simulation* (2003) **2**, 62.